PROCEEDINGS OF ECOS 2023 - THE 36TH INTERNATIONAL CONFERENCE ON
EFFICIENCY, COST, OPTIMIZATION, SIMULATION AND ENVIRONMENTAL IMPACT OF ENERGY SYSTEMS
25-30 JUNE 2023, LAS PALMAS DE GRAN CANARIA, SPAIN

Numerical Multiphase assessment of geometric key parameters in Venturi-type reactor for process intensification

Nicola Andreini[a], Guglielmo Vaccaro[a], Luca Socci[a],Adriano Milazzo[a]

[a] Department of industrial Engineer University of Florence, Florence, Italy.
Corresponding author: nicola.andreini@unifi.it

Abstract:
Hydrodynamics cavitation has the potential to significantly improve the efficiency and effectiveness of a wide range of industrial processes, including water treatment, chemical reactions, food processing, and biomass pretreatment. Cavitation can be used to replace traditional processing methods that are more energy-intensive or use harmful chemicals, which can help to increase the sustainability of industrial processes. Overall, using cavitation for process intensification can help improve efficiency, sustainability, and circularity in industry. One of the most used device that is easy to integrate with the production line is the cavitating Venturi reactor. In the present work, influence of the key geometric parameters such as the height and length of Venturi throat are evaluated to find the optimum reaction conditions enhancing cavitating treatment intensity and minimizing the pressure drop. The analysis has been conducted by varying the ratio of the throat section to the inlet section, keeping constant the cavitation number, to have cavitation dependent only on the geometry. A series of multiphase simulations have been performed using an open-source solver (OpenFOAM) that implements the Zwart-Gerber-Belamri cavitation model. The adopted modelling approach was the VOF (volume of fluid) mixture type coupled with the URANS (Unsteady Reynolds Averaged Navier Stokes) method, in which a komegaSST turbulence model has been applied. An FFT analysis was conducted to evaluate the cavitation regime. It was observed that by increasing the throat diameter, the frequency of the re-entrant jet mechanism decreases while the cavitation region extends. Finally the impact of pressure drop in various geometries was evaluated and compared with the CEP (cavitation efficiency parameter), a term developed to properly evaluate the efficiency of the cavitation phenomenon.

Keywords:
CFD, multiphase, cavitation, process intensification , energy saving.

1. Introduction

Hydrodynamic cavitation has gained a strong interest in recent years for its unique features, versatility, and effectiveness in many fields. Among them, it is possible to mention waste wastewater treatment and biofuel production [1]. In wastewater treatment, hydrodynamic cavitation represents a useful help to achieve high standards of depuration. Generally speaking, standard wastewater treatments aim to reduce the concentration of certain pollutants. Biological treatments are widely used, but they are not completely effective on constituents persistent to biodegradation, which undergo only minor structural changes in absence of additional treatments [2]. Moreover, the widespread diffusion of high-environment impact industrial processes, that produce new kinds of pollutants, has accentuated this fact [3]. So, in the context of wastewater treatments, there is a necessity to apply specific processes able to reduce the presence of these pollutants. In this sense, cavitation can be considered a very promising option, eventually coupled with advanced techniques (such as Advanced Oxidation Processes, AOP). Indeed, the so high values of pressure (up to a GigaPascal range) and temperature (in the order of 10 000 K) are suited for all the mechanisms of degradation of biological and chemical compounds [2]. In the hydrodynamic cavitation phenomenon applied to wastewater treatment, all consequences deriving from bubbles collapse are employed [4]: thermal, mechanical and chemical effects. The thermal effects include temperature gradient and temperature rise rate, which are beneficial to damage the structure of pathogens and to assist other removal mechanisms. The intensive mechanical effect breaks the outer structures of pathogens, inactivating them. The chemical effects are determined by the breaking of water molecules, leading to the formation of strongly oxidising radicals: hydroxyl OH and hydrogen peroxide -OH 2, which are highly effective on persistent pollutants. The real effectiveness of hydrodynamic cavitation on various species of water pollutants depends on the operating parameters and specific design of cavitating reactors [1], [3], [4]. Moreover, the combined use of hydrodynamic cavitation with other advanced oxidation processes has been proposed [3], [[5]. Regarding biofuels, hydrodynamic cavitation can be employed to enhance the production of biodiesel and bioethanol. In particular, bioethanol production is based on the availability of a

https://doi.org/10.52202/069564-0043

sugar matrix, that could derive from sugar/starch crops (1st generation bioethanol) or lignocellulosic plants (2nd generation). The latter has gained particular attention because it does not need dedicated crops. This process relies on some pretreatments aiming to change the supramolecular structure of biomass in which the cellulose, lignin and hemicellulose are closely interconnected to finally release free sugars making them available for the next transformation (fermentation, distillation, refining) [6], [7]. In this regard, hydrodynamic cavitation can be used as a pre-treatment for delignification, effectively and with energy savings compared to traditional technologies. Results obtained in several tests indicate that pre-treatment with hydrodynamic cavitation leads to excellent ethanol production yields and a high degree of ethanol purity [8] For extensive industrial uses, hydrodynamic cavitation (HC), produced by accelerated flow, is well suited [9].When compared to other generation techniques like optic, acoustic, and particle, HC has the benefits of good scalability, simplicity of manufacture, and a promising treatment outcome. The geometric design of the cavitating device has a significant impact on cavitation intensity like operating pressure, flow rate, etc. Numerous devices have been investigated as cavitating reactor for process intensification, including orifices, venturi, vortex diodes, etc. Even so, there are still gaps in the knowledge of cavitating flow through these devices, particularly the cavitating venturi, despite its simplicity and widespread use. The design methods for a cavitating reactor currently used are mostly empirical and have no optimization criteria that can increase the yield of the process to which cavitation is applied. Another gap in the literature is the lack of an unambiguous term for evaluating the efficiency of a cavitating device. Various methods, based on experiments, for assessing cavitation intensity have been proposed, for example, Dastane et al. [11] estimated the efficiency of the cavitation process by introducing a parameter called Cavitational Efficacy Ratio (CER), the ratio between pressure generated after cavity collapse and pressure losses. The collapse pressure reflects the greatest quantity of energy that a cavity can release when collapsing. Wu et al. [10] developed a formulation for the energy released during the cavitation phenomenon to quantify its intensity. Other works attempt to give a formulation for cavitation efficiency however for engineering purposes they are very complex and difficult to use on an industrial scale. From the aforementioned literature, it is clear that stronger cavitation causes higher effects on process intensification. This connection is straightforward and natural. In this paper, various key parameters are analyzed to evaluate which one is the best in terms of optimization of cavitation performance and pressure loss minimization. To evaluate the impact of the geometry, 2D axisymmetric simulations taken from the literature have been used. Next, a cavitation model based on the Rayleight-Plesset equations developed by Zwar-Belamri-Gerber [16] and a modification for turbulent viscosity proposed by Delgosha [19] was implemented in a multiphase solver available in OpenFOAM software. After validating the model on a literature test case taken from Stutz-Reboud [12], sensitivity analysis was performed on the cavitating device.

2. Numerical Model

To simulate the phenomenon of cavitation, an unsteady solver of the OpenFOAM has been adopted. The solver was modified appropriately to increase the accuracy of the results. The chosen solver is designed to simulate the phenomenon of cavitation for an incompressible, isothermal, and immiscible fluid. It adopts a VOF mixtures (Volume of fluid) approach with an interface capturing method proposed by Hirt and Nichols [14]in which a single set of governing equations is defined for the two liquid-vapour phases. The Reynolds-averaged Navier stokes equations in their unsteady formulation for Newtonian fluids have been considered, than the conservative equations of mass, momentum, and the transport equation for the volume fraction α, used to solve the interface between liquid and vapour, can be written as:

$$\frac{\partial \rho_m}{\partial t} + \nabla \cdot (\rho_m \mathbf{U}) = 0 \tag{1}$$

$$\frac{\partial (\rho_m U)}{\partial t} + \nabla \cdot (\rho_m \mathbf{U}\mathbf{U}) = -\nabla P + \nabla \cdot [\mu_{eff}(\nabla \mathbf{U} + (\nabla \mathbf{U})^T)] + f_\sigma + \rho_m g \tag{2}$$

$$\frac{\partial \alpha_v}{\partial t} + \nabla \cdot \mathbf{U} + \nabla \cdot [\mathbf{U}\mathbf{c}\alpha_v(1-\alpha_v)] = S_\alpha \tag{3}$$

Where μ_{eff} represents the sum of molecular viscosity and turbulent viscosity, S_α The term due to the amount of evaporation and condensation rates, f_σ is the surface tension force acting at the liquid-vapour interface while the third LHS term of the transport equation of volume fraction is called as artificial compression term, which is not zero only at the interface. This contribution is important because using a VOF approach with a purely convective α equation would lead to numerical diffusion and thus in a non-conservative interface. The generic fluid property is instead calculated as a weighted average over the volume fraction of the individual properties

https://doi.org/10.52202/069564-0043

of the two liquid-vapour phases. For the fluid was considered Newtonian although someone to be treated may exhibit different behavior because a general treatment has been conducted. The specific response of cavitating fluids, whether it leads to a suppression or enhancement of non-Newtonian behavior, depends on the rheological properties of the fluid, such as its viscosity, elasticity, yield stress, and the specific conditions of the cavitation process, including pressure, flow velocity, and geometry. The properties of the individual phases were calculated using REFPROP software and were considered constant, as in most of the work in the literature:

$$\phi_m = (1 - \alpha_v)\phi_l + \phi_v\alpha_v \tag{4}$$

To model the phase change effects due to the cavitation phenomenon, the Zwart-Gerber- Belamri (ZGB) [16] model based on the Rayleigh-Plesset equations has been implemented: it describes the behaviour of the single cavitation bubble in space and time. By simplifying the terms due to surface tension, the second-order derivatives, liquid viscosity, and non-condensable gas, the relationship between the change in the bubble radius and the pressure become:

$$\frac{dR}{dt} = \sqrt{\frac{2(P_v - P)}{3\rho_l}} \tag{5}$$

From this equation it is possible to express the evaporation and condensation rates and derive the source terms to be included in the transport equation [3]. Considering spherical bubbles of radius R_B , with a density per cell equal to n, it is possible to write:

$$\alpha_v = n(\frac{4}{3}\pi(R_B)^3) \tag{6}$$

From here, combining equations 6 and 5, after some mathematical steps it is possible to derive the formulation of the sink terms of evaporation and condensation proposed by [16]:

$$\dot{S}_\alpha = \begin{cases} F_v \frac{3r_{nuc}(1-\alpha_v)\rho_v}{R_B}\sqrt{\frac{2}{3}\frac{P_{sat}-P}{\rho_l}} & \text{if } P < P_{sat} \\ F_{\text{cond}}\ \frac{3r_v\alpha_v}{R_B}\sqrt{\frac{2}{3}\frac{P-P_{sat}}{\rho_l}} & \text{if } P > P_{sat} \end{cases} \tag{7}$$

where $r_{nuc} = 5x10^{-4}$ is the nucleation site volume fraction, $R_B = 10^{-6}[m]$ nucleation site radius and $F_v = 50$, $F_{cond} = 0.01$ empirical calibration constants. These model parameters were set as proposed by ZBG. For turbulence modelling, a k-omega SST (Shear Stress Transport) was proposed by Menter [17]. As suggested by the work of Chebli, Delgosha et Al. [13] modification for turbulent viscosity was added in order to simulate unsteady behaviour of cavitating flow [Equation 8,9]. The model uses two transport equations: one for the turbulent kinetic energy k and another for the specific dissipation rate of turbulent kinetic energy omega. The k equation accounts for the production and dissipation of turbulence, while the omega equation accounts for the transport and destruction of turbulence. The SST model uses a blending function for a smooth transition between a near wall low-Reynolds number model and a far field high-Reynolds number model. Other turbulence models, such as the Reynolds Stress Model or the Large Eddy Simulation, may also be appropriate for certain cavitation applications.

$$\mu_t = f(\rho)a_1\frac{k}{\max(a_1\omega, b_1F_{23}\mathbf{S})} \tag{8}$$

$$f(\rho) = \frac{\rho_v + \alpha_l^n(\rho_l - \rho_v)}{\rho_v + \alpha_l(\rho_l - \rho_v)} \tag{9}$$

A wall-resolved approach was chosen for the wall boundary layer. For this reason, the grid was built to have a Y^+ less than 5, as is usually done in the literature. Regarding unsteady cavitation flows, it has been observed in the literature that standard turbulence models cannot correctly predict the oscillatory behaviour of the flow. The turbulent viscosity is a key parameter in turbulence models that describes the rate at which turbulent energy is dissipated into heat. In cavitating flows, the presence of vapour bubbles can cause significant changes in the

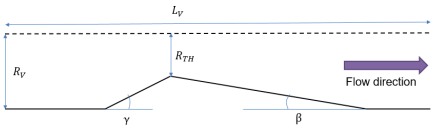

Figure 1: schematic view of nozzle geometry where L_V = 340mm is the lenght of entire domain, R_{TH} and L_{TH} = 10mm are the radius and lenght of the throath, R_V = 50mm radius of the channel and γ = 22.5°- β = 6° are the convergent and divergent angle.

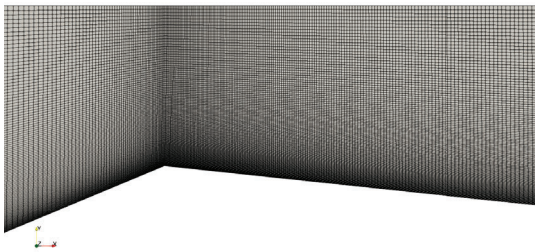

Figure 2: View of 2D axisymmetric computational mesh in which the grid thickening in the near-wall and cavitation region can be observed.

turbulent viscosity due to the highly compressible nature of the vapour phase. As is reported in the literature turbulent viscosity is overestimated in the cavitation region, since most turbulent models are not sensitive to phase change. This causes an inhibition of the phenomenon of cavitating bubble cluster shedding that affects the correct numerical prediction. For this reason, a correcting function [eq 9] developed by Delgosha [19], a modification to standard turbulence models that aims to account for the effects of cavitation on the turbulent viscosity, was implemented. The value of n is fixed to 10 as suggested by Delgosha et al. [19]

3. Geometry and numerical setup

For sensitivity analysis on the influence of throat cross-section on the phenomenon of cavitation, a Venturi-type reactor studied by Long et al. [15] was taken as a test case. The chosen geometry is shown in [Figure 1]. To prevent the length of the throat from having an impact in the simulations, we decided to remove it and use a sharp edge. As pointed out by the work of Ulla et al. [18] , the absence of the throat section, increases cavitation length. The domain for the simulation was realized by an axisymmetric structured 2D mesh shown in the figure 2 , consisting of about 100k hexahedral elements. In the regions near the wall, the mesh was refined and a wall resolved approach was adopted. For numerical simulations, 4 geometries were chosen in which the convergent and divergent ramp angles were kept constant and the throat height was varied: 5-10-15-20 mm. Boundary conditions represent a crucial aspect for simulations of cavitation phenomena since the development of the cavitation generates numerous pressure oscillations that spread within the channel, both upstream and downstream. For this reason to avoid pressure fluctuations and possible spurious solutions, two stitches were added, one downstream and one upstream of the venturi nozzle. The following boundary condition is used: an imposed velocity at the inlet equal to 0.89 m/s (in agreement with experimental data where the reference flow rate was imposed equal to 1.74 L/s), a static pressure set at the outlet equal to 200k Pa that was selected to reproduce the pressure value at the inlet measured from experimental data. One of the most widely used dimensionless parameters to study cavitation phenomena is the cavitation number, which takes into account the pressure drop in the fluid and the kinetic energy of the fluid, which are the two main factors that influence the behaviour of cavitation, and is defined as:

$$\sigma = \frac{P_{out} - P_{sat}}{\frac{1}{2}\rho U_{TH}^2} \tag{10}$$

where P_{out} represents the pressure imposed at the outlet, P_{sat} the fluid saturation pressure calculated at a temperature of 19°, U_{TH} the average velocity in the throat section. To evaluate the effects of throat diameter on the development of the cavitation region, which is a useful effect for process intensification, and to study the

https://doi.org/10.52202/069564-0043

Table 1: list of numerical models and schemes

Parameter/variable/name	*Model/Scheme*
Multiphase model	Eulerian–Eulerian VOF
Volume fraction	parameters Implicit scheme
Viscous model	$k-\omega SST$
Cavitation model	Zwart-Gerber- Belamri
ThermoPhisical Properties	constant
Spatial discretization-Gradient	Gauss linear
Spatial discretization-Momentum	Second order upwind
Spatial discretization-Volume fraction	Gauss VanLeer
Spatial discretization-Turbulent kinetic energy	Second order upwind
Spatial discretization-Specific dissipation rate	Second order upwind
Transient formulation	Second Order Backward

behaviour of pressure drop, 4 geometries were created. For the generation of the geometries, the convergent and divergent ramp angles were kept constant, while for the boundary conditions, both the outlet pressure and the throat velocity were kept constant by varying the inlet velocity to obtain the same cavitation number value (shown in table 2). A second-order numerical schemes for both time and other variables has been used, and in addition, the PIMPLE algorithm was used for solving governing equations, while the MULES algorithm (semi-implicit and second order in time) was used to ensure that the volume fraction (alpha) remains between strict bounds of 0 and 1. Regarding computational settings, we chose a time step $TS = 10^{-7}[s]$ to ensure a $CFL < 0.7$.

Table 2: Values used for sensitivity analysis on the influence of throat section in the cavitation process

$D_{TH}(mm)$	$U_{in}(m/s)$,	σ
5	0.223	0.8
10	0.89	0.8
15	2	0.8
20	3.55	0.8

4. Result

4.1. Re-entrant jet mechanism

the unsteady phenomena governing cavitation are mainly two:

- Shock front mechanism in which a shock front is formed in a certain region of the cavitation zone and moving upstream causes vapour condensation.
- Re-entrant jet mechanism is a pressure driven mechanism in which a vortex causes the detachment of a cavitating cluster that is carried downstream by the flow.

For all simulations, we observe that only the re-entrant jet mechanism is present. To investigate the influence of geometry in terms of re-entrant jet mechanism and shedding frequency, virtual probes are located on the axis in the control section near the inlet. In figures 3 and 4 show the dynamics of the re-entrant jet mechanism and the pressure signal obtained from the simulation of the Venturi device having a throat diameter of 10 mm. From point A to point E the cavitation zone grows until the re-entrant jet is created and cavitating cell detachment occurs. Subsequently attached sheet cavity decrease until disappears (point H). Starting from here we have three pressure spikes related to points (G to I), where the cavity breakoff takes place. This is the first cycle of the cavity shedding mechanism. After that, at point (L) the appearance of a new cavitating region, marking the beginning of the secondary cycle with pressure peaks less intense than in the first cycle happens. Once the cavity that was generated in the first cycle collapses the shedding phenomenon ends (Q) and the pressure values return to those of state A.

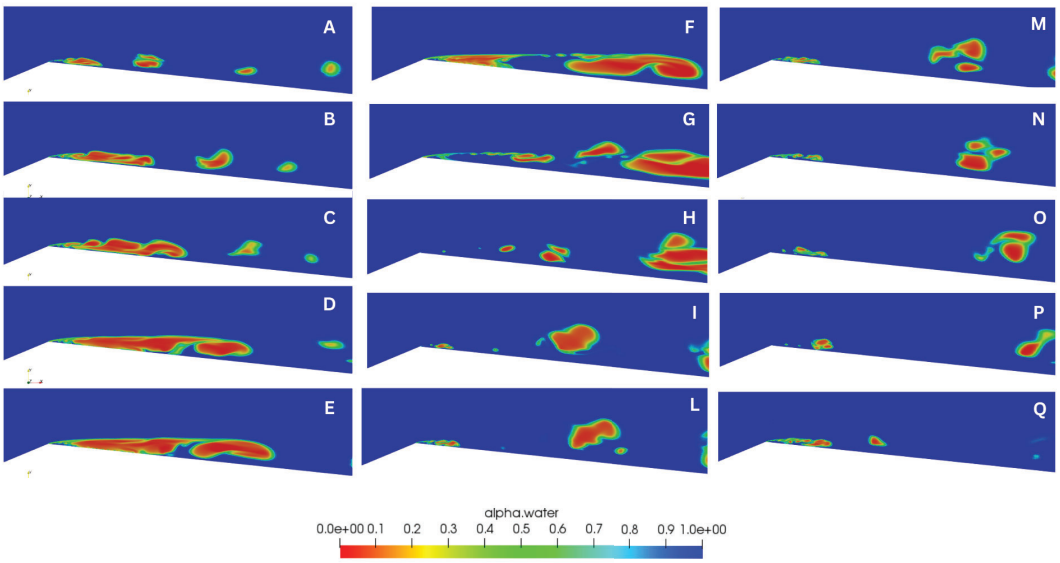

Figure 3: Re-entrant jet cycles in a Venturi device with D_{TH} = 10mm. From point A to H the first cycle of the re-entrant jet mechanism, characterized by an extended cavitation region, is shown. From I to L can be notices the second cycle in which the extension of cavity is smaller that the first.

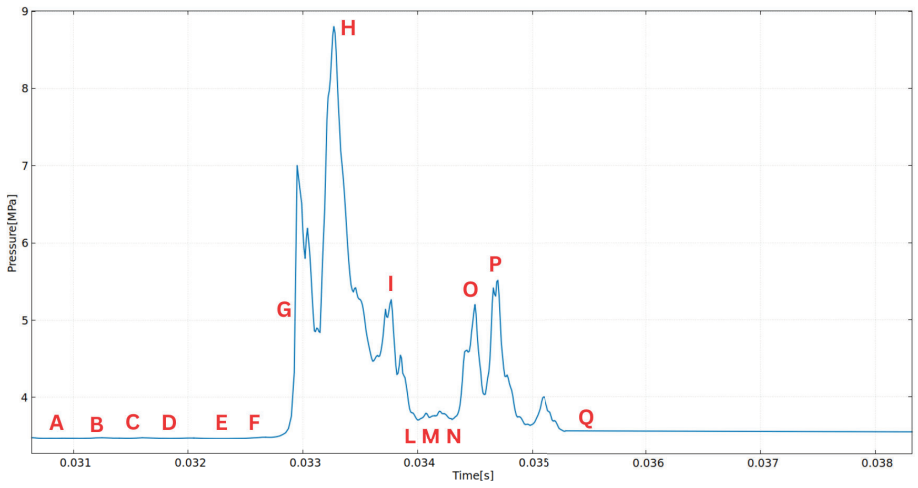

Figure 4: Pressure behaviour calculated at the inlet section in a Venturi device with D_{TH} = 10mm

Using the FFT fast Fourier transform 5, it was possible to analyze the characteristic frequencies of the re-entrant jet phenomenon of the four simulated geometries. At smaller throat cross sections, the frequency of the system increases while the pressure peaks associated with the breakoff of the cavities decrease. As reported in a later section, this behaviour is associated with the formation of a cavities in the first shedding cycle. Downstream of the throat, the pressure recovery is more gradual for larger diameters, this causes the life of the cavitating cells to increase (the collapse position is moved downstream), this lead to dwindle of frequency. The oscillation period increases. Geometries with larger throat cross sections showed higher oscillation, both in terms of frequency and flow rate. This is something to investigate as it could be an undesirable effect for the system in which the cavitating device will be installed.

https://doi.org/10.52202/069564-0043

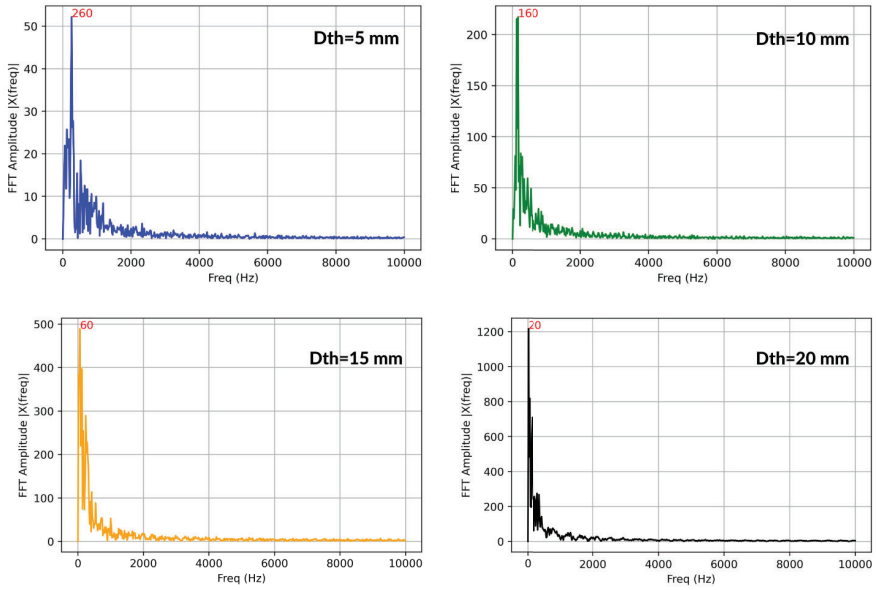

Figure 5: Result from FFT analysis, the number in red represents the frequency of the system .

4.2. Evaluation of overall cavitation efficiency

From the simulations obtained, it was possible to calculate parameters related to cavitation efficiency (length of cavitation, the value of volume fraction at certain stations and amplitude of the cavitating region) and parameters related to pressure drop with which an optimized geometry could be chosen. For this purpose, it has been developed a term called cavitation efficiency parameter (CEP) for evaluating cavitation efficiency that takes into account the average volume occupied by cavities:

$$CEP = \frac{\sum_{i=0}^{n}[V_i \alpha_{Vi}]}{\pi D_{in} \frac{D_{TH}^2}{4}} \tag{11}$$

where V_i is the volume of i-th cell , α_{Vi} is the value of vapour volume fraction in the i-th cell, n is the number of cells, while D_{TH} is the throat diameter. The ratio represents a weighted average over the volume fraction of the cavitating volume and a cylinder having diameter equal to D_{TH} and height equal to the channel's diameter D_{in}. To calculate CEP a python code that takes as input the results obtained from the simulations and returns the value of CEP was developed. This parameter is very fast and simple to be obtained and can be easily integrated into the design process of the cavitating device. Then the value of pressure losses over the entire nozzle was calculated, defined as:

$$K = \frac{\Delta P}{\frac{1}{2}\rho U_{TH}^2} \tag{12}$$

where ΔP is the difference between total pressure at the inlet and outlet while U_{TH} is the throat velocity. These two parameters were used to compare the various simulations and estimate the influence of the throat section on the cavitation process. Time average Volume fraction fields are shown in figure 6 for the four geometries. It can be seen that as the diameter increases, the cavitation region becomes larger. The lengths of the average cavitating region for the various geometries are given in Table 3 while the plot of K and CEP are shown in fig. 7. From the results obtained, it can be seen that at the same cavitation number both losses and CEP have a favourable trend for larger diameters. The best configuration seems to be that for DTH = 20mm in which the cavitation volume increases while the losses decrease as the main flow has less blocking effect due to the cavitating region.

https://doi.org/10.52202/069564-0043

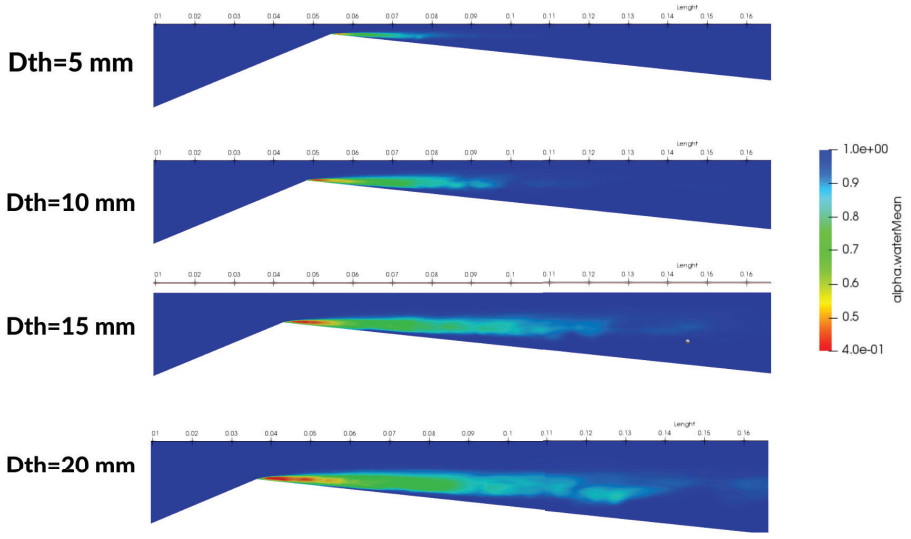

Figure 6: Time average liquid volume fraction for simulated geometry.

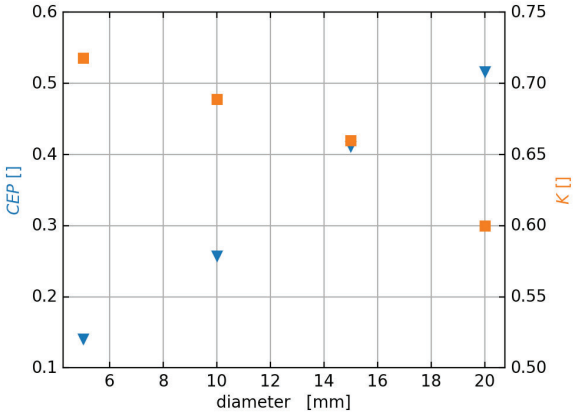

Figure 7: The graph shows the trend of K losses and CEP as a function of throat diameter.

4.3. Effect of throat length in cavitating flow dynamics

This section analyzes the differences in terms of the dynamics of the cavitation phenomenon between a sharp-edged geometry and a geometry in which there is a throat section of length L_{TH}. It has been decided to consider the geometry with $D_{TH} = 10mm$ and $L_{TH} = 10mm$. Once the simulations were finished, it was possible to evaluate the differences between the two geometries using the FFT and calculating both the K losses and the cavitating efficiency parameter. The presence of the throat region causes the emergence of a quasi-stable sheet cavity region, which causes a clear decrease in the oscillation period. In terms of frequency, we have a reduction from 160 Hz for the sharp-edged to 40 Hz for the geometry in which the throat region is present. While the amplitude related to the pressure spike remains almost the same (Figure 9). Regarding the velocity field, the presence of two recirculation zones located at the beginning of the throat section and at the beginning of the diverging ramp is observed in figure 10. The instabilities that are generated at the sheet cavity interface, tend to energize the flow in the second recirculation zone. This results in an inhibition of the cavitation phenomenon which is therefore less intense than having a sharp-edged throat. The performance for process intensification values of CEP = 0.17 while the losses give a value of K = 0.58. Compared with the values found for the sharp-edged geometry, it is observed that CEP decreases given the smaller extent of the cavitation region. Pressure losses, directly related to the extent of the cavitation region where the largest contributions of pressure degradation are shown, also decreasing from 0.689 to 0.58.

https://doi.org/10.52202/069564-0043

Table 3: Lenght of cavitation region measured from the throat to the point of maximum abscissa with liquid volume fraction equal to 0.95.

$D_{TH}(mm)$	$L_{cav}(mm)$
5	23
10	46
15	79
20	97

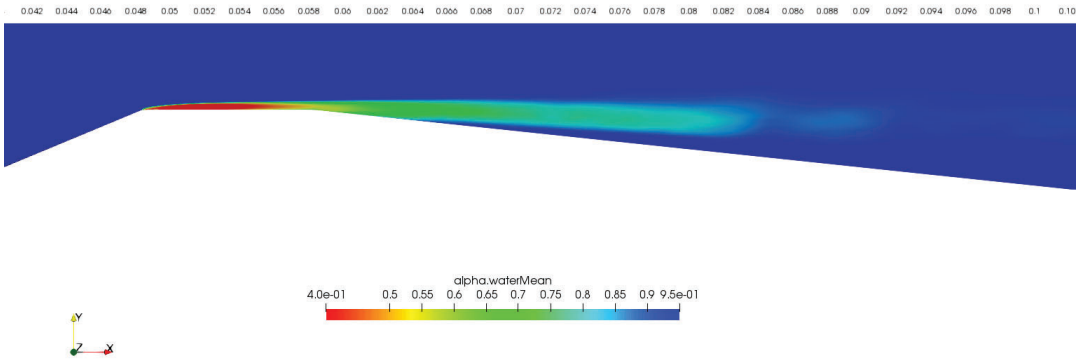

Figure 8: Average volume fraction of geometry with cavitating lenght of 10 mm, in the throat section there is presence of quasi stable sheet cavity.

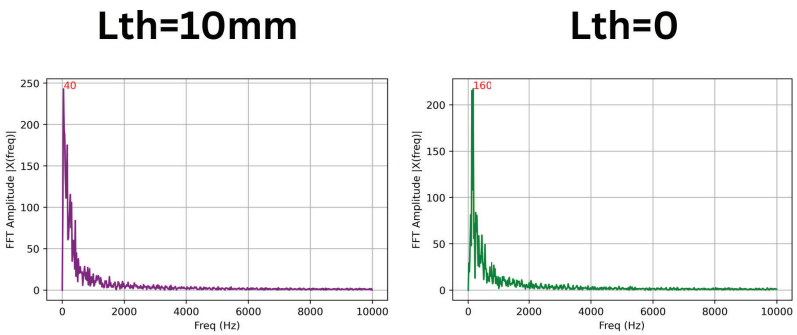

Figure 9: FFT Fast Fourier Transform for evaluate the effect of throat lenght in cavitation dynamics behaviour.

5. Conclusion

In this paper, the influence of the throat section on the cavitation process for process intensification was investigated. It is understood that the unsteady process of cavitation is very complex and it depends on many factors. Using an FFT analysis it was possible to study the phenomenon of the re-entrant jet mechanism and

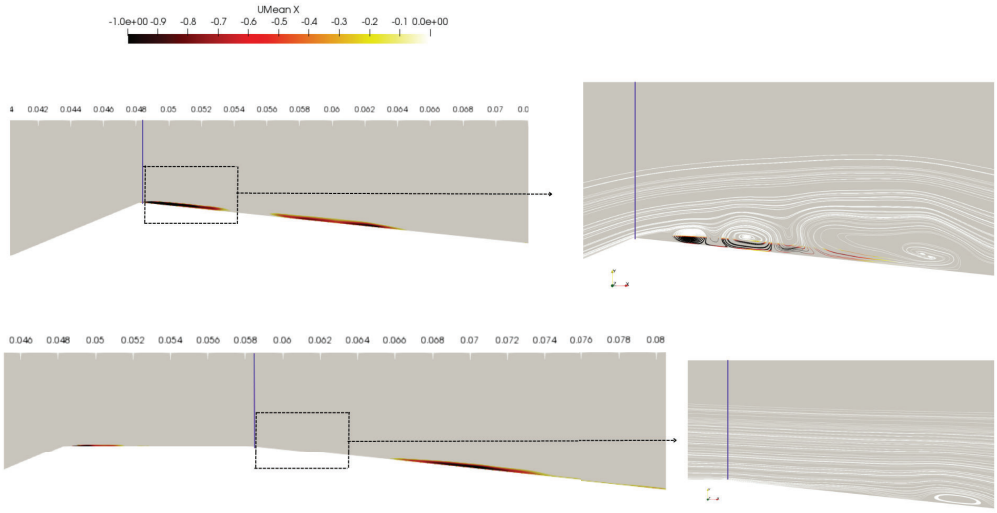

Figure 10: Average velocity field in which are compared the recirculation zone, the purple line represent the downstream throat section. On the left the streamline of the flow are plotted.

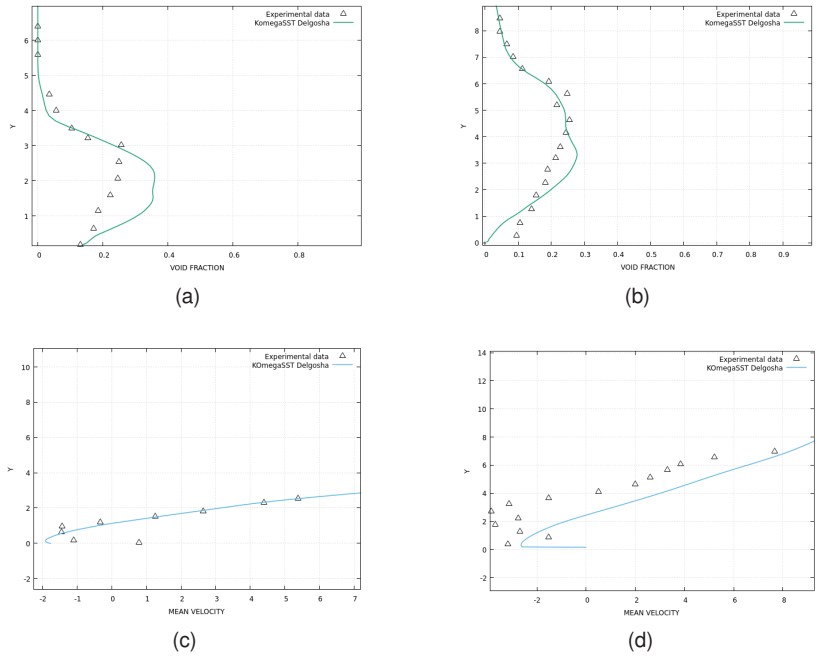

Figure 11: Stutz Reboud test case [12]: a comparison between experimental data across the cavity at the station 1 and 2 and time-avarage numerical simulation. on the top a) b) show the mean volume fraction profile while on the bottom c) d) show the mean velocity field.

was found that an increase in throat section leads to a decrease in the oscillation frequency of cavities while a decrease in throat leads to a reduction in cavitation region extension. Despite the simplicity of the venturi device, there is no parameter to evaluate the effectiveness of the reactor for process intensification. For this reason, a specific term was developed to evaluate cavitation efficiency that was compared to the pressure drop within the cavitating device. Further experimental or numerical studies, are needed to determine the effect of varying the pressure at the outlet and keeping the same mass flow rate on the cavitation behaviour (at

https://doi.org/10.52202/069564-0043

a constant cavitation number). This forms the scope of future work.

Appendix A Model Validation

One of the critical aspects of cavitation models is to obtain reliable and accurate results. This is because especially empirical models or those based on Rayleigh-Plesset equations need a careful calibration process from the point of view of the numerical schemes and simulation settigs. from the point of view of the numerical schemes. For this work, since we do not have experimental data of the momentum field and volume fraction trend for the chosen geometry, we considered one of the most widely used test cases in the literature (Stutz and Reboud [12]) [12]) that offers experimental data on both the velocity field and volume fraction profile in the cavitation zone. Numerical settings are the same as those mentioned in the numerical setup section while a mesh of 100K hexahedral elements was made for the geometry. From the comparisons with the experimental data shown in graph 11, it can be seen that there is good agreement with the volume fraction and velocity profiles calculated with the developed model. The only differences are found at the first station where the mean value of volume fraction is overestimated, showing an inaccuracy in simulating the sheet cavitation region. While at the second station it is noticeable that the velocity profile calculated with cfd tends to underestimate the recirculation region. This is due to the URANS model used, in fact such models fail to totally capture adverse pressure gradients. A more detailed study of the velocity profile can be done using high fidelity approaches to evaluate the interaction between cavitating flow and turbulence. Comparison with experimental data showed how there is an error of about 4 percent in the calculation of cavitation length (48mm with numerics and 50 mm from experiment). For these reasons, the model was considered as validated.

Nomenclature

- D Diameter [m]
- f_σ surface tension [N/m]
- K Pressure losses
- k Turbulent kinetic energy [J/Kg]
- L Lenght [m]
- L_V total Venturi's Lenght [m]
- P pressure [Pa]
- R_B bubble radius [m]
- R_V Channel radius[m]
- S_α evaporation/condensation source term [kg/m^4]
- V volume [m^3]
- t time [s]
- T temperature, [°C]
- U velocity [m/s]

Greek symbols

- α volume fraction
- β divergent angle [DEG]
- γ convergent angle [DEG]
- ω specific dissipation rate [1/s]
- μ_{eff} effective viscosity [Ns]
- ρ density [kg/m^3]
- ϕ generic function

Subscripts and superscripts

in	inlet section
m	mixture
out	outlet section
sat	saturation
TH	Throat
v	vapour
w	water

References

[1] . Wang, H. Su, and B. Zhang, *'Hydrodynamic cavitation as a promising route for wastewater treatment – A review', Chemical Engineering Journal, vol. 412, p. 128685, May 2021, doi: 10.1016/j.cej.2021.128685.*

[2] . Dular et al., *'Use of hydrodynamic cavitation in (waste) water treatment', Ultrasonics Sonochemistry, vol. 29, pp. 577–588, Mar. 2016*

[3] R. Darandale, M. V. Jadhav, A. R. Warade, and V. S. Hakke, *'Hydrodynamic cavitation a novel approach in wastewater treatment: A review', Materials Today: Proceedings, p. S2214785322074478, Dec. 2022.*

[4] Y. Song, R. Hou, W. Zhang, and J. Liu, *'Hydrodynamic cavitation as an efficient water treatment method for various sewage:- A review', Water Science and Technology, vol. 86, no. 2, pp. 302–320, Jul. 2022*

[5] B. Wang et al., *'Hydrodynamic cavitation and its application in water treatment combined with ozonation: A review', Journal of Industrial and Engineering Chemistry, vol. 114, pp. 33–51, Oct. 2022*

[6] F. Verdini, E. Calcio Gaudino, G. Grillo, S. Tabasso, and G. Cravotto, *'Cellulose Recovery from Agri-Food Residues by Effective Cavitational Treatments', Applied Sciences, vol. 11, no. 10, p. 4693, May 2021*

[7] Sun et al., *'Recent advances in hydrodynamic cavitation-based pretreatments of lignocellulosic biomass for valorization', Bioresource Technology, vol. 345, p. 126251, Feb. 2022*

[8] Kim, I. Lee, S. H. Jeon, T. Hwang, and J.-I. Han, *'Hydrodynamic cavitation as a novel pretreatment approach for bioethanol production from reed', Bioresource Technology, vol. 192, pp. 335–339, Sep. 2015.*

[9] Ivakumar, Manickam, Siah Ying Tang, and Khang Wei Tan.*S "Cavitation technology–a greener processing technique for the generation of pharmaceutical nanoemulsions." Ultrasonics sonochemistry 2014.*

[10] Wu, Pengfei, Lixin Bai, and Weijun Lin. *On the definition of cavitation intensity. Ultrasonics Sonochemistry.*

[11] Dastane, Gaurav G., et al. *Single and multiphase CFD simulations for designing cavitating venturi. Chemical Engineering Research and Design 149 (2019): 1-12.*

[12] Stutz, B., and J. L. Reboud. *Experiments on unsteady cavitation. Experiments in fluids 22.3 (1997): 191-198.*

[13] Chebli, R., B. Audebert, G. Zhang, and O. Coutier-Delgosha. *Influence of the turbulence modeling on the simulation of unsteady cavitating flows. Computers Fluids 221 (2021): 104898.*

[14] Hirt, C.W.; Nichols, B.D. *Volume of fluid (VOF) method for the Dynamics of Free Boundaries. J. Comput. Phys. 1981, 39, 201–225.*

[15] Long, Xinping, et al. *"Experimental investigation of the global cavitation dynamic behavior in a venturi tube with special emphasis on the cavity length variation." International Journal of Multiphase Flow.*

[16] Zwart, Philip J and Gerber, Andrew G and Belamri, Thabet and others - *Two-phase flow model for predicting cavitation dynamics , Fifth international conference on multiphase flow, Yokohama 2004.*

[17] F.R. Menter, R. Langtry, and S. Volker. *Transition Modelling for General Purpose CFD Codes. Flow, Turbulence and Combustion 2006.*

[18] Ullas, P. K., Dhiman Chatterjee, and S. Vengadesan. *"Experimental study on the effect of throat length in the dynamics of internal unsteady cavitating flow." Physics of Fluids 35.2 (2023): 023332.*

[19] Coutier-Delgosha, Olivier and Fortes-Patella, Regiane and Reboud, Jean-Luc *Evaluation of the turbulence model influence on the numerical simulations of unsteady cavitation - J. Fluids Eng. 2003.*

https://doi.org/10.52202/069564-0043